M. Morandini
A Two-Level Nonlinear Beam Analysis Method
International Journal of Solids and Structures, Vol. 203, 2020, p. 224-235
doi:10.1016/j.ijsolstr.2020.08.003

A two-level nonlinear beam analysis method

Marco Morandini[a,*]

[a]*Politecnico di Milano, Dipartimento di Scienze e Tecnologie Aerospaziali, via La Masa 34, 20156 Milano, ITALY*

Abstract

The nonlinear response of straight, constant cross section beams is investigated by means of a two-level finite element solution procedure. The higher level model is built starting from the Hellinger-Reissner principle, with the normal stress resultant and moment resultant as additional unknowns field beside the beam reference line position and orientation field. A lower-level nonlinear cross-section problem is defined for each integration point. The two-level models are linked together by the normal stress resultant and moment resultant, in one direction, and by the variation of the complementary strain energy in the other: the cross-section level do deform in such a way that the the normal stress resultant and moment resultant are equal to those of the beam model, while the higher level beam model receives the gradient and Hessian of the complementary strain energy with respect to the resultants. The complementary strain energy gradient and Hessian are computed by defining suitable first and second order adjoint problems.

Keywords: two-level, beam, cross section, nonlinear, plasticity, Taylor expansion

*Corresponding author.
Email address: marco.morandini@polimi.it (Marco Morandini)

1. Introduction

When dealing with slender structures a beam model allows to drastically reduce the number of unknowns with respect to those of a three dimensional model. Most of the time a beam is designed in such a way that the material response will be linear elastic, even if the overall structural response is nonlinear. This allows to characterize the response of the beam cross-section once for all by computing the cross-section stiffness matrix, a linear relationship between resultant and moment resultant of the the normal stress vector and the beam generalized strain measures. Countless papers deal with this characterization problem. Among them, the Taylor expansion proposed by Ieşan (1976) is worth mentioning, see also Ieşan (2008) and its application for the characterization of functionally graded beam cross-sections by Bîrsan et al. (2012); the first general numerical approach for the characterization of an arbitrary beam cross-section was perhaps developed by Giavotto et al. (1983); the early paper by Berdichevsky (1981) inspired the variational asymptotic approach, extensively developed by Hodges (2006, and references therein) and his co-workers; an Hamiltonian setting (cfr. Mielke, 1991; Druz et al., 1996; Zubov, 2006; Romanova and Ustinov, 2008) is instead at the basis of the approach developed by Morandini et al. (2010) and later on by Han and Bauchau (2015). In some sense, a beam model is always a two-level model; the lower level solution, however, is often computed once for all.

Whenever the material response departs from linear elasticity it is clearly no more reasonable to compute the cross-section stiffness matrix once for all. Jiang and Yu (2015) extended the variationally asymptotic method to

account for nonlinear material response when the beam is subject to constant axial force, torsion and bending, but not for shear, that would entail linearly varying bending moment. A similar approach, but not limited to constant internal actions was recently proposed by Morandini (2019). Other approaches are available as well, often based on simple kinematic assumptions for the cross section motion and/or on the assumption of an axial stress state; in this regards, the works of Rigobello et al. (2013), Rezaiee-Pajand and Gharaei-Moghaddam (2015) and Chiorean (2017) are worth mentioning.

Bilotta and Garcea (2019) proposed linking their version of the cross-section characterization procedure (Genoese et al., 2014a,b) to a nonlinear beam model, thus building a two-level nonlinear beam analysis framework; the link is performed by transferring the increment of the generalized strains of the beam model, evaluated at the beam element control points, to the cross-section model, and searching for the increment of beam warping that allows satisfying the local equilibrium equations at the cross-section level; after this it is then possible to compute the resultant and moment resultant of the cross-section normal stress vector, that are needed by the beam model. Their proposal is limited to small strains, thought.

This paper proposes a two-level nonlinear beam analysis framework that links the nonlinear cross-section analysis proposed by Morandini (2019) to a nonlinear beam model. The link is built in a variationally sound way, with the global beam response guaranteed to remain hyperelastic if the beam material is hyperelastic. Typical FE^2 multilevel approaches gives as input to the lower level model the macroscale strain tensor, and get back from the lower level model the average stress tensor. Here, instead, the resultant and moment

resultant of the cross-section normal stress vector are passed as input from the beam model to the lower-level cross-section model; the beam model, in turn, gets back the generalized deformations and their derivatives with respect to the normal stress resultant and moment resultant. A Hellinger-Reissner two-field variational principle is used for the beam model; this allows to have, among the higher level model unknowns, the resultants and moment resultants of the normal stress vector. As an added bonus, this choice allows to prevent shear locking.

The outline of the paper is as follows. Section 2 details the proposed formulation. Section 3 is dedicated to few selected examples. The run time requirements of the proposed two-level method are briefly discussed within Section 4. The conclusions of Section 5 close the paper.

2. Formulation

The proposed formulation is the subject of this section, that is split into four Subsections. The first Subsection 2.1 briefly reviews the intrinsic non-linear beam model used within this work, and the corresponding Hellinger-Reissner two-field variational principle; Subsection 2.2 summarizes the non-linear cross-section analysis procedure proposed in Morandini (2019). Subsection 2.3 details how the models of Subsection 2.1 and 2.2 can be combined into a two-level method. Subsection 2.4 provides the missing link from the low-level cross-section model to the beam model, explaining how first and second adjoint problems of the cross-section model allow to compute the first and second variations of the cross-section complementary strain energy.

2.1. Beam model

A beam intrinsic model is defined as a one-dimensional polar continuum; in other words, a beam is represented by a line whose configuration is described, in the deformed configuration, by the position vector $\boldsymbol{x}'(s)$ and by the orientation tensor $\boldsymbol{\alpha}'(s)$ at a point, with $\boldsymbol{\alpha}'$ a orthogonal unit tensor and s the arc length in the reference configuration. At any given point the beam is able to transmit an internal force $\boldsymbol{T}$ and an internal moment $\boldsymbol{M}$. Vectors $\boldsymbol{T}$ and $\boldsymbol{M}$ are understood to be the resultant and moment resultant, computed over the cross section of a slender prismatic three dimensional solid, of the normal stress vector. Following e.g. Pietraszkiewicz and Eremeyev (2009); Cardona and Geradin (1988); Merlini and Morandini (2013) a pair of generalized linear and angular strain measures $\hat{\boldsymbol{\epsilon}}$ and $\hat{\boldsymbol{\beta}}$ can be defined as

$$\begin{aligned} \hat{\boldsymbol{\epsilon}} &= \boldsymbol{\alpha}'^T \boldsymbol{x}'_{,s} - \boldsymbol{\alpha}^T \boldsymbol{x}_{,s} \\ \hat{\boldsymbol{\beta}} &= \boldsymbol{\alpha}'^T \mathrm{ax}(\boldsymbol{\alpha}'^T \boldsymbol{\alpha}'_{,s}) - \boldsymbol{\alpha}^T \mathrm{ax}(\boldsymbol{\alpha}^T \boldsymbol{\alpha}_{,s}) \end{aligned} \tag{1}$$

where $\boldsymbol{x}(s)$ and $\boldsymbol{\alpha}(s)$ are the position and orientation tensors in the reference configuration and the ax() operator extracts the vector characterizing a skew-symmetric tensor, so that $\mathrm{ax}(\boldsymbol{B}) \times \boldsymbol{c} = \boldsymbol{B}\boldsymbol{c}$ for any skew symmetric tensor $\boldsymbol{B}$ and vector $\boldsymbol{c}$. These strain measures are work-conjugated the back-rotated resultant and moment resultant vectors

$$\begin{aligned} \hat{\boldsymbol{T}} &= \boldsymbol{\alpha}'^T \boldsymbol{T} \\ \hat{\boldsymbol{M}} &= \boldsymbol{\alpha}'^T \boldsymbol{M} \end{aligned} \tag{2}$$

so that the internal virtual work per unit length of the beam model is equal to $(\delta\hat{\boldsymbol{\epsilon}}\hat{\boldsymbol{T}} + \delta\hat{\boldsymbol{\beta}}\hat{\boldsymbol{M}})$, and the one-field principle of virtual work reads

$$\int_l \left(\delta\hat{\boldsymbol{\epsilon}}\hat{\boldsymbol{T}} + \delta\hat{\boldsymbol{\beta}}\hat{\boldsymbol{M}}\right) \mathrm{d}s - \delta L_e = 0, \tag{3}$$

with δL_e the virtual work of the external loads. The force and moment vectors $\hat{\boldsymbol{T}}$ and $\hat{\boldsymbol{M}}$ can be assumed to be function of the generalized strains $\hat{\boldsymbol{\epsilon}}$ and $\hat{\boldsymbol{\beta}}$.

Assume the existence of a strain energy function $w(\hat{\boldsymbol{\epsilon}}, \hat{\boldsymbol{\beta}})$ per unit of length such that $\delta w = \hat{\boldsymbol{T}}\delta\hat{\boldsymbol{\epsilon}} + \hat{\boldsymbol{M}}\delta\hat{\boldsymbol{\beta}}$, $\hat{\boldsymbol{T}} = w_{,\hat{\boldsymbol{\epsilon}}}$ and $\hat{\boldsymbol{M}} = w_{,\hat{\boldsymbol{\beta}}}$. It is thus possible to take its Legendre transform and define the complementary strain energy v, function of $\hat{\boldsymbol{T}}$ and $\hat{\boldsymbol{M}}$,

$$v(\hat{\boldsymbol{T}}, \hat{\boldsymbol{M}}) = \hat{\boldsymbol{\epsilon}}\hat{\boldsymbol{T}} + \hat{\boldsymbol{\beta}}\hat{\boldsymbol{M}} - w \tag{4}$$

such that $\delta v = \hat{\boldsymbol{\epsilon}}\delta\hat{\boldsymbol{T}} + \hat{\boldsymbol{\beta}}\delta\hat{\boldsymbol{M}}$ and $\hat{\boldsymbol{\epsilon}} = v_{,\hat{\boldsymbol{T}}}$ $\hat{\boldsymbol{\beta}} = v_{,\hat{\boldsymbol{M}}}$. The Hellinger-Reissner two-field variational principle can then be readily derived as

$$\begin{aligned} &\mathcal{H}(\delta\hat{\boldsymbol{\epsilon}}, \delta\hat{\boldsymbol{\beta}}, \delta\hat{\boldsymbol{T}}, \delta\hat{\boldsymbol{M}}, \hat{\epsilon}, \hat{\boldsymbol{\beta}}, \hat{\boldsymbol{T}}, \hat{\boldsymbol{M}}) = \\ &\int_l \left(\delta\hat{\boldsymbol{\epsilon}}\hat{\boldsymbol{T}} + \delta\hat{\boldsymbol{\beta}}\hat{\boldsymbol{M}} + \delta\hat{\boldsymbol{T}}\hat{\epsilon} + \delta\hat{\boldsymbol{M}}\hat{\boldsymbol{\beta}} - \delta v(\hat{\boldsymbol{T}}, \hat{\boldsymbol{M}})\right) \mathrm{d}s - \delta L_e = 0, \end{aligned} \tag{5}$$

where $\boldsymbol{x}'$, $\boldsymbol{\alpha}'$, $\hat{\boldsymbol{T}}$ and $\hat{\boldsymbol{M}}$ are independent unknowns and the linear form $\mathcal{H}$ must be equal to zero for any compatible variation of the test functions. Here the strains $\hat{\boldsymbol{\varepsilon}}$ and $\hat{\boldsymbol{\beta}}$, and their variations, are known functions of $\boldsymbol{x}'$, $\boldsymbol{\alpha}'$ and their variations, cfr. Eq. 1. Traditional, intrinsic beam models do need a constitutive law for computing the internal force and moment resultants as a function of their work-conjugated deformations. This constitutive law is almost always defined starting from the de Saint-Venant's solutions of

the three dimensional body, see e.g. Giavotto et al. (1983); Hodges (2006); Morandini et al. (2010) and references therein.

2.2. Cross section model

In a recent paper Morandini (2019) has shown how to locally approximate, at a given cross-section, the nonlinear three dimensional solution of a slender prismatic body, loaded only at its extremities, as a function of the internal force and moment resultants $\hat{\boldsymbol{T}}$ and $\hat{\boldsymbol{M}}$. This can be accomplished without the need to solve the boundary problem for the whole structure. The local approximation is the basis of the lower lever model used in this work, and is briefly summarized in the following.

Assume the cross-section to lie onto the x, y, plane, with $\boldsymbol{i}^1$, $\boldsymbol{i}^2$ and $\boldsymbol{i}^3$ the unit vectors along the x, y and z axis, respectively. The principle of virtual work reads

$$\int_V \delta \boldsymbol{F} : \hat{\boldsymbol{S}} dV = \int_A \delta \hat{\boldsymbol{x}}' (L) \cdot \boldsymbol{f} (L) \, \mathrm{d}A + \int_A \delta \hat{\boldsymbol{x}}' (0) \cdot \boldsymbol{f} (0) \, \mathrm{d}A \tag{6}$$

where $\boldsymbol{F}$ is the deformation gradient, $\hat{\boldsymbol{S}}$ is the first Piola-Kirchhoff stress tensor and the right hand side represents the virtual work of the loads applied at the two beam extremities, located at $z = 0$ and $z = L$. The deformation gradient $\boldsymbol{F}$ can be decomposed in its in-plane and out-of-plan components

$$\boldsymbol{F} = \mathrm{grad}_S(\hat{\boldsymbol{x}}') + \hat{\boldsymbol{x}}'_{,z} \otimes \boldsymbol{i}^3, \tag{7}$$

where $\hat{\boldsymbol{x}}'$ is the deformed position vector and $\mathrm{grad}_S(\hat{\boldsymbol{x}}') = \hat{\boldsymbol{x}}'_{,x} \otimes \boldsymbol{i}^1 + \hat{\boldsymbol{x}}'_{,y} \otimes \boldsymbol{i}^2$. Integration by part of the left hand side with respect to z leads to

$$\begin{aligned} &- \int_L \int_A \delta \hat{\boldsymbol{x}}' \otimes \boldsymbol{i}^3 : \hat{\boldsymbol{S}}_{,z} \mathrm{d}A \mathrm{d}z + \int_L \int_A \delta \mathrm{grad}_S(\hat{\boldsymbol{x}}') : \hat{\boldsymbol{S}} \mathrm{d}A \mathrm{d}z + \\ &+ \left[\int_A \delta \hat{\boldsymbol{x}}' \cdot \left(\hat{\boldsymbol{S}} \cdot \boldsymbol{n} - \boldsymbol{f} \right) \mathrm{d}A \right]_L + \left[\int_A \delta \hat{\boldsymbol{x}}' \cdot \left(\hat{\boldsymbol{S}} \cdot \boldsymbol{n} - \boldsymbol{f} \right) \mathrm{d}A \right]_0 = 0. \end{aligned} \tag{8}$$

where $\boldsymbol{n}$ if the outward-pointing unit normal (i.e. $\boldsymbol{n} = \boldsymbol{i}^3$ for $z = L$ and $\boldsymbol{n} = -\boldsymbol{i}^3$ for $z = 0$), the first two integral do represent the equilibrium equations along the beam and the last two integrals are the weak form of the Newmann boundary conditions at the two beam extremities $z = 0$ and $z = L$. Thus, the equilibrium along the beam is satisfied if

$$-\int_A \delta\hat{\boldsymbol{x}}' \otimes \boldsymbol{i}^3 : \hat{\boldsymbol{S}}_{,z} \mathrm{d}A + \int_A \delta \mathrm{grad}_S(\hat{\boldsymbol{x}}') : \hat{\boldsymbol{S}} \mathrm{d}A = 0. \tag{9}$$

The objective here is to find a local polynomial approximation of the solution at $z = 0$. To do so, the displacement $\hat{\boldsymbol{u}} = \hat{\boldsymbol{x}}' - \hat{\boldsymbol{x}}$, with $\hat{\boldsymbol{x}}$ the position vector in the reference configuration, is s approximated around $z = 0$ as

$$\hat{\boldsymbol{u}}(x, y, z) \approx \sum_{i=0}^{N} \frac{1}{i!} \hat{\boldsymbol{u}}_i(x, y) z^i, \tag{10}$$

where the unknown field $\hat{\boldsymbol{u}}_i(x, y)$, a function of the cross section position only, is the i-th displacement derivative of field $\hat{\boldsymbol{u}}(x, y, z)$ wrt. z evaluated at $z = 0$. Eq. 9, evaluated at $z = 0$ is not sufficient to close the problem; to do so one needs to account for its derivatives, up to order N, with e.g. its first derivative given by

$$\begin{aligned} &-\int_A \delta\hat{\boldsymbol{x}}'_{,z} \otimes \boldsymbol{i}^3 : \hat{\boldsymbol{S}}_{,z} \mathrm{d}A - \int_A \delta\hat{\boldsymbol{x}}' \otimes \boldsymbol{i}^3 : \hat{\boldsymbol{S}}_{,zz} \mathrm{d}A + \\ &\int_A \delta \left(\mathrm{grad}_S \hat{\boldsymbol{x}}'\right)_{,z} : \hat{\boldsymbol{S}} \mathrm{d}A + \int_A \delta \mathrm{grad}_S \hat{\boldsymbol{x}}' : \hat{\boldsymbol{S}}_{,z} \mathrm{d}A = 0. \end{aligned} \tag{11}$$

Four additional constraints are required as well. The first two require that the cross- section stress resultant and moment resultant, computed at $z = 0$, should be equal to the sought values $\hat{\boldsymbol{T}}$ and $\hat{\boldsymbol{M}}$

$$\begin{aligned} \textstyle\int_A \hat{\boldsymbol{S}} \cdot \boldsymbol{i}^3 \mathrm{d}A &= \hat{\boldsymbol{T}}, \\ \textstyle\int_A \hat{\boldsymbol{x}}' \times \hat{\boldsymbol{S}} \cdot \boldsymbol{i}^3 \mathrm{d}A &= \hat{\boldsymbol{M}}; \end{aligned} \tag{12}$$

the last two set of equations constraint the average displacement and rotation of the cross section

$$\begin{aligned} &\int_A \hat{\boldsymbol{u}}_0 \mathrm{d}A = \mathbf{0}, \\ &\int_A \hat{\boldsymbol{x}} \times \hat{\boldsymbol{u}}_0 \mathrm{d}A = \mathbf{0}. \end{aligned} \tag{13}$$

Eqs. 12 and 13 are imposed by means of four Lagrange multiplier vectors $\boldsymbol{\lambda}_j$, $j \in [1, 4]$. The whole set of nonlinear equations will be referred to, in the sequel, as

$$\mathcal{F}(\delta\hat{\boldsymbol{u}}_i, \delta\boldsymbol{\lambda}_j, \hat{\boldsymbol{u}}_i, \boldsymbol{\lambda}_j, \{\hat{\boldsymbol{T}}, \hat{\boldsymbol{M}}\}) = 0 \tag{14}$$

where $\boldsymbol{u}_i$ and $\boldsymbol{\lambda}_j$ are the unknowns, $i \in [1, N]$, $j \in [1, 4]$, $\delta\boldsymbol{u}_i$ and $\delta\boldsymbol{\lambda}_j$ are the test functions and $\{\hat{\boldsymbol{T}}, \hat{\boldsymbol{M}}\}$, the sought cross-section internal actions, are two independent vector parameters forcing the system. The linear form $\mathcal{F}$ must be equal to zero for any compatible variation of the test functions; furthermore, it is linear not only with respect to the test functions, but also with respect to $\hat{\boldsymbol{T}}$ and $\hat{\boldsymbol{M}}$. Different approximation schemes can, in principle, be chosen for the unknown fields $\hat{\boldsymbol{u}}_i(x, y)$. Among them, standard or isogeometric finite elements. Standard finite elements and a Galerkin method were chosen in Morandini (2019) to numerically solve the problem $\mathcal{F} = 0$, with the test function defined by $\delta\boldsymbol{u} = \sum_{i=0}^{N} \frac{1}{i!}\delta\boldsymbol{u}_i(x, y)z^i$, and $\delta\boldsymbol{u}_i(x, y)$ resorting to the same cross-section approximation adopted for the unknown fields $\boldsymbol{u}_i$. The same choice is taken here.

It is worth noting that it would not be possible to find an equilibrium configuration that solves the nonlinear cross-section problem of Eq. 14 should the sought internal actions $\{\hat{\boldsymbol{T}}, \hat{\boldsymbol{M}}\}$ exceed the cross-section limit load.

2.3. Two-level scheme

The beam model of Section 2.1 can be used to solve any beam nonlinear problem, but needs an inverse constitutive law, allowing to compute the variation of the complementary strain energy per unit of reference length v with respect to the variation of the cross section normal stress resultant and moment resultant $\hat{\boldsymbol{T}}$ and $\hat{\boldsymbol{M}}$; these resultant vectors are among the unknowns of the problem $\mathcal{H} = 0$ defined with Eq. 5. Conversely, the local approximation of Section 2.2 allows to approximate the nonlinear response of the beam around a given cross section as a function of the the cross section normal stress resultant and moment resultant vectors, $\hat{\boldsymbol{T}}$ and $\hat{\boldsymbol{M}}$, that act as forcing terms for the nonlinear cross-section model equations $\mathcal{F} = 0$ of Eq. 14. A two-level scheme can be built by resorting to both models and feeding the resultant and moment resultant vectors $\hat{\boldsymbol{T}}$ and $\hat{\boldsymbol{M}}$ of the beam model into the local model. By doing so the local model is used to predict the cross-section response as a function of the cross section internal actions of the beam model, and can feed back to the beam model the first and second variation of the cross section complementary strain energy per unit of reference length with respect to the internal actions themselves.

Note that the internal action vectors $\hat{\boldsymbol{T}}$ and $\hat{\boldsymbol{M}}$ of the beam model are back-rotated into the cross-section reference system, cfr. Eq. 2. The initial orientation $\boldsymbol{\alpha}$ of the beam model should thus be defined in such a way that the beam cross-section, back rotated by $\boldsymbol{\alpha}$, is brought into the cross section of the local model. This allows to consistently match the back-rotated internal actions $\hat{\boldsymbol{T}}$ and $\hat{\boldsymbol{M}}$ of Eq. 2 with the normal stress resultant and moment resultant vectors of Eq. 12.

This procedure is exemplified in Figure 1: a given, slender solid, solid, a) in the Figure, is idealized by the beam model b), encompassing a reference line with a structure and, implicitly, a constitutive law derived from an analysis performed at the cross-section level. This idealized model can be approached at two levels. The first one, c), is global, and leads to a finite element approximation of the Hellinger-Reissner principle $\mathcal{H} = 0$. The second one, d) is at the cross-section level, and leads to a finite-element approximation of the nonlinear problem $\mathcal{F} = 0$. Different local models are defined, one for each integration point of the global model. For each integration point of the global model the internal actions values can be fed, as forcing parameters, to the corresponding local model, so that the local nonlinear problem $\mathcal{F} = 0$ can be solved for the sought values of the internal actions; after having reached convergence with the cross-section local problem it is then possible to compute the first derivative of the cross-section complementary strain energy $\mathrm{d}v/\mathrm{d}\{\hat{\boldsymbol{T}}, \hat{\boldsymbol{M}}\}$ and, if required, its Hessian $\mathrm{d}^2v/\mathrm{d}\{\hat{\boldsymbol{T}}, \hat{\boldsymbol{M}}\}^2$ as well. These two derivatives are what is required to assemble the residual vector $\mathcal{H}$ of the global problem and its Jacobian matrix. The procedures for computing the complementary strain energy derivatives are detailed in Section 2.4.

It is worth stressing once more that the complementary strain energy derivatives of a given local cross-section model can be computed only after having reached convergence, $\mathcal{F} = 0$. This means that the local nonlinear problem needs to be solved, up to convergence, for every iteration of the higher level beam model solution procedure, because the unknown internal action vectors $\hat{\boldsymbol{T}}$ and $\hat{\boldsymbol{M}}$ may keep changing. In other words, a local model has not really reached a converged configuration, even if $\mathcal{F} = 0$, unless the

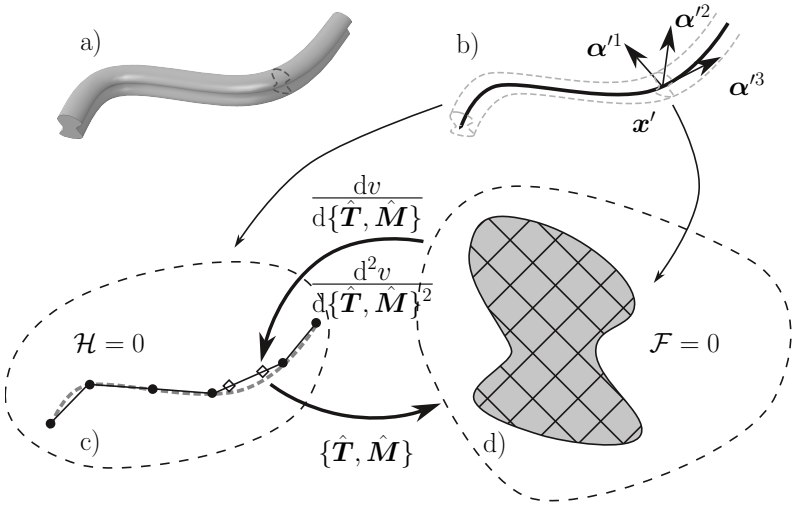

Figure 1: Interaction between the global beam and local cross-section models.

beam model has converged as well. In practice, if the local model accounts for plasticity (or for any other irreversible material behavior) then the state from which the flow rules are integrated from can be changed only after having reached the convergence of the both the local and the global model, $\mathcal{F}=0$ and $\mathcal{H}=0$, and not when $\mathcal{F}=0$ but $\mathcal{H}\neq 0$.

2.4. Cross-section complementary strain energy derivatives

Assume a material characterized by an internal energy per unit of reference volume at constant temperature $\psi(\boldsymbol{\epsilon},\boldsymbol{\chi})$, where $\boldsymbol{\epsilon}=\frac{1}{2}(\boldsymbol{F}^T\boldsymbol{F}-\boldsymbol{I})$ is the Green-Lagrange strain tensor, and $\boldsymbol{\chi}$ stands for whatever internal hidden variables may be required to describe possibly irreversible material behaviors. Let the Second Piola-Kirchhoff stress tensor $\boldsymbol{S}$, that is work-conjugated with $\boldsymbol{\epsilon}$, be given by $\boldsymbol{S}=\psi_{,\boldsymbol{\epsilon}}$. The integral over of the cross section of the Legendre transform $\boldsymbol{S}:\boldsymbol{\epsilon}-\psi(\boldsymbol{F},\boldsymbol{\chi})$ allows to compute the complementary

strain energy v per unit of beam length:

$$v = \int_A \boldsymbol{S} : \boldsymbol{\epsilon} - \psi(\boldsymbol{\epsilon}, \boldsymbol{\chi}) \mathrm{d}A \tag{15}$$

For the local model the functional v, that can be computed as a function of the unknown displacement functions $\hat{\boldsymbol{u}}_i$, is constrained by the equilibrium equations $\mathcal{F}(\delta\boldsymbol{u}, \boldsymbol{u}, \{\hat{\boldsymbol{T}}, \hat{\boldsymbol{M}}\}) = 0$ where $\boldsymbol{u}$ includes both the unknown functions $\hat{\boldsymbol{u}}_i$ and the Lagrangian multiplier vectors $\boldsymbol{\lambda}_j$. This means that, after having solved the cross-section problem $\mathcal{F} = 0$ for for some given $\{\hat{\boldsymbol{T}}, \hat{\boldsymbol{M}}\}$ and having found the unknown functions $\hat{\boldsymbol{u}}_i$, the complementary strain energy can be considered as a pure function of vectors $\{\hat{\boldsymbol{T}}, \hat{\boldsymbol{M}}\}$ themselves, say $\hat{v}(\{\hat{\boldsymbol{T}}, \hat{\boldsymbol{M}}\}) = v(\hat{\boldsymbol{u}}_i(\{\hat{\boldsymbol{T}}, \hat{\boldsymbol{M}}\}))$. The local model need to compute the first and second derivative of the complementary strain energy Eq. 15 with respect to the internal actions $\{\hat{\boldsymbol{T}}, \hat{\boldsymbol{M}}\}$. To do so, it is possible to resort to a well-known technique based on adjoint equations, see e.g. Hinze et al. (2008). The actual implementation for the computation of the Hessian of $\hat{v}$ was heavily inspired by code snippets found within the dolfin-adjoint library, see Farrell et al. (2013) and Mitusch et al. (2019) for details. Here the formulæ are particularized for the case at hand. Since $\hat{\boldsymbol{u}}_i$ are understood to be a function of $\{\hat{\boldsymbol{T}}, \hat{\boldsymbol{M}}\}$ we have

$$\frac{\mathrm{d}\hat{v}}{\mathrm{d}\{\hat{\boldsymbol{T}}, \hat{\boldsymbol{M}}\}} = v_{,\boldsymbol{u}} \boldsymbol{u}_{,\{\hat{\boldsymbol{T}}, \hat{\boldsymbol{M}}\}} \tag{16}$$

where

$$\begin{aligned} v_{,\boldsymbol{u}} &= \int_A \boldsymbol{\epsilon} : \boldsymbol{S}_{,\boldsymbol{\epsilon}} : \boldsymbol{\epsilon}_{,\boldsymbol{u}} + \boldsymbol{S} : \boldsymbol{\epsilon}_{,\boldsymbol{u}} - \psi_{,\boldsymbol{\epsilon}} : \boldsymbol{\epsilon}_{,\boldsymbol{u}} \mathrm{d}A \\ &= \int_A \boldsymbol{\epsilon} : \boldsymbol{S}_{,\boldsymbol{\epsilon}} : \boldsymbol{\epsilon}_{,\boldsymbol{u}} \mathrm{d}A \end{aligned} \tag{17}$$

because $\psi_{,\boldsymbol{\epsilon}} = \boldsymbol{S}$. The derivative of $\boldsymbol{u}$ with respect to $\{\hat{\boldsymbol{T}}, \hat{\boldsymbol{M}}\}$ can be computed by deriving the cross-section equations $\mathcal{F} = 0$:

$$\frac{\mathrm{d}\mathcal{F}}{\mathrm{d}\{\hat{\boldsymbol{T}}, \hat{\boldsymbol{M}}\}} = \mathcal{F}_{,\boldsymbol{u}}\boldsymbol{u}_{,\{\hat{\boldsymbol{T}},\hat{\boldsymbol{M}}\}} + \mathcal{F}_{,\{\hat{\boldsymbol{T}},\hat{\boldsymbol{M}}\}} = 0 \tag{18}$$

from which

$$\boldsymbol{u}_{,\{\hat{\boldsymbol{T}},\hat{\boldsymbol{M}}\}} = -\mathcal{F}_{,\boldsymbol{u}}^{-1}\mathcal{F}_{,\{\hat{\boldsymbol{T}},\hat{\boldsymbol{M}}\}} \tag{19}$$

where the partial derivatives of $\mathcal{F}$ with respect to the components of $\{\hat{\boldsymbol{T}}, \hat{\boldsymbol{M}}\}$, $\mathcal{F}_{,\{\hat{\boldsymbol{T}},\hat{\boldsymbol{M}}\}}$, are trivial to compute, since $\mathcal{F}$ is linear with respect to the forcing parameters $\{\hat{\boldsymbol{T}}, \hat{\boldsymbol{M}}\}$, cfr. Eq. 12. Computing the derivatives of $\boldsymbol{u}$ with respect to $\{\hat{\boldsymbol{T}}, \hat{\boldsymbol{M}}\}$, $\boldsymbol{u}_{,\{\hat{\boldsymbol{T}},\hat{\boldsymbol{M}}\}}$, would however require the solution of six linear systems. The solution of these linear system can be avoided, at least for computing the first derivative of $\hat{v}$. Replacing Eq. 19 into Eq. 16, leads to

$$\frac{\mathrm{d}\hat{v}}{\mathrm{d}\{\hat{\boldsymbol{T}}, \hat{\boldsymbol{M}}\}} = -v_{,\boldsymbol{u}}\mathcal{F}_{,\boldsymbol{u}}^{-1}\mathcal{F}_{,\{\hat{\boldsymbol{T}},\hat{\boldsymbol{M}}\}}; \tag{20}$$

it is now possible to define the vector of adjoint variables $\boldsymbol{\lambda}_A$ such that

$$\boldsymbol{\lambda}_A^T = v_{,\boldsymbol{u}}\mathcal{F}_{,\boldsymbol{u}}^{-1}. \tag{21}$$

The adjoint variables can thus be computed as the solution of the linear system

$$\boldsymbol{\lambda}_A^T\mathcal{F}_{,\boldsymbol{u}} = v_{,\boldsymbol{u}}. \tag{22}$$

Re-writing Eq. 20 as a function of the adjoint variables $\boldsymbol{\lambda}_A$ leads to the sough result

$$\frac{\mathrm{d}\hat{v}}{\mathrm{d}\{\hat{\boldsymbol{T}}, \hat{\boldsymbol{M}}\}} = -\boldsymbol{\lambda}_A^T\mathcal{F}_{,\{\hat{\boldsymbol{T}},\hat{\boldsymbol{M}}\}}. \tag{23}$$

The overall computational cost is that of the solution of a single sparse linear system, Eq. 22, with the same number of unknowns of the local problem $\mathcal{F} = 0$.

The second derivative of v with respect to the k-th component of $\{\hat{\boldsymbol{T}}, \hat{\boldsymbol{M}}\}$, i.e. the k-th row of $\frac{\mathrm{d}^2\hat{v}}{\mathrm{d}\{\hat{\boldsymbol{T}},\hat{\boldsymbol{M}}\}^2}$, can be computed by deriving Eq. 23:

$$\left(\frac{\mathrm{d}^2\hat{v}}{\mathrm{d}\{\hat{\boldsymbol{T}}, \hat{\boldsymbol{M}}\}^2}\right)_{(k,:)} = -\frac{\mathrm{d}\boldsymbol{\lambda}_A^T}{\mathrm{d}\{\hat{\boldsymbol{T}}, \hat{\boldsymbol{M}}\}_{(k)}}\mathcal{F}_{,\{\hat{\boldsymbol{T}},\hat{\boldsymbol{M}}\}} \tag{24}$$

where $\frac{\mathrm{d}\boldsymbol{\lambda}_A^T}{\mathrm{d}\{\hat{\boldsymbol{T}},\hat{\boldsymbol{M}}\}_{(k)}}$ is the derivative of $\boldsymbol{\lambda}_A^T$ with respect to the k-th component of $\{\hat{\boldsymbol{T}}, \hat{\boldsymbol{M}}\}$ and the second derivative $\mathrm{d}(\mathcal{F}_{,\{\hat{\boldsymbol{T}},\hat{\boldsymbol{M}}\}})/\mathrm{d}\{\hat{\boldsymbol{T}}, \hat{\boldsymbol{M}}\}_{(k)}$, that should appear in Eq. 24, is null because $\mathcal{F}$ is linear with respect to $\{\hat{\boldsymbol{T}}, \hat{\boldsymbol{M}}\}$ and its derivative $\mathcal{F}_{,\{\hat{\boldsymbol{T}},\hat{\boldsymbol{M}}\}}$ is not function of $\boldsymbol{u}$, cfr. Eq. 12. The derivative $\frac{\mathrm{d}\boldsymbol{\lambda}_A^T}{\mathrm{d}\{\hat{\boldsymbol{T}},\hat{\boldsymbol{M}}\}_{(k)}}$ can be computed by deriving Eq. 22

$$\frac{\mathrm{d}\boldsymbol{\lambda}_A^T}{\mathrm{d}\{\hat{\boldsymbol{T}}, \hat{\boldsymbol{M}}\}_{(k)}}\mathcal{F}_{,\boldsymbol{u}} + \boldsymbol{\lambda}_A^T(\mathcal{F}_{,\boldsymbol{uu}}\boldsymbol{u}_{,k}) = v_{,\boldsymbol{uu}}\boldsymbol{u}_{,k} \tag{25}$$

where $\boldsymbol{u}_{,k}$ stands for the derivative of $\boldsymbol{u}$ with respect to the k-th component of $\{\hat{\boldsymbol{T}}, \hat{\boldsymbol{M}}\}$, and can be computed from Eq. 19; the second partial derivative $\mathcal{F}_{,\boldsymbol{u}k}$ of $\mathcal{F}$ with respect to $\boldsymbol{u}$ and to the k-th component of $\{\hat{\boldsymbol{T}}, \hat{\boldsymbol{M}}\}$ does not appear in Eq. 25 because the derivative of $\mathcal{F}$ with respect to $\{\hat{\boldsymbol{T}}, \hat{\boldsymbol{M}}\}$ does not depend on $\boldsymbol{u}$, cfr. Eq. 12. Since $\boldsymbol{u}_{,k}$ and $\boldsymbol{\lambda}_A$ can be computed independently Eq. 25 is nothing but a linear system of equations with $\frac{\mathrm{d}\boldsymbol{\lambda}_A^T}{\mathrm{d}\{\hat{\boldsymbol{T}},\hat{\boldsymbol{M}}\}_{(k)}}$ as unknown:

$$\frac{\mathrm{d}\boldsymbol{\lambda}_A^T}{\mathrm{d}\{\hat{\boldsymbol{T}}, \hat{\boldsymbol{M}}\}_{(k)}}\mathcal{F}_{,\boldsymbol{u}} = v_{,\boldsymbol{uu}}\boldsymbol{u}_{,k} - \boldsymbol{\lambda}_A^T(\mathcal{F}_{,\boldsymbol{uu}}\boldsymbol{u}_{,k}) \tag{26}$$

After solving Eq. 26 for $\frac{\mathrm{d}\boldsymbol{\lambda}_A^T}{\mathrm{d}\{\hat{\boldsymbol{T}},\hat{\boldsymbol{M}}\}_{(k)}}$ the k-th row of $\frac{\mathrm{d}^2\hat{v}}{\mathrm{d}\{\hat{\boldsymbol{T}},\hat{\boldsymbol{M}}\}^2}$ is readily given by Eq. 24. The computation of $\frac{\mathrm{d}^2\hat{v}}{\mathrm{d}\{\hat{\boldsymbol{T}},\hat{\boldsymbol{M}}\}^2}$ requires the solution of twelve linear systems: for each row of $\frac{\mathrm{d}^2\hat{v}}{\mathrm{d}\{\hat{\boldsymbol{T}},\hat{\boldsymbol{M}}\}^2}$ one needs to solve a linear system for computing $\boldsymbol{u}_{,k}$ from Eq. 19, and an additional linear system for computing $\frac{\mathrm{d}\boldsymbol{\lambda}_A^T}{\mathrm{d}\{\hat{\boldsymbol{T}},\hat{\boldsymbol{M}}\}_{(k)}}$ from Eq. 26. One also needs to compute the first order adjoint

variables $\boldsymbol{\lambda}_A$ from Eq. 22, but this usually brings no additional cost, since they are required in order to compute the first order derivative of $\hat{v}$.

It is worth noting that the matrix of the cross-section complementary strain energy second derivatives with respect to the stress resultant and moment resultant vectors, $\hat{\boldsymbol{T}}$ and $\hat{\boldsymbol{M}}$, is nothing but the generalized cross-section compliance matrix of an initially straight beam, with its inverse leading the the cross-section tangent stiffness matrix. As such, it is a generalization of the linear characterization procedures of e.g. Giavotto et al. (1983), Hodges (2006) and Bîrsan et al. (2012).

3. Examples

Within all the examples the global beam model adopts a continuous linear interpolation for the displacement and rotation fields, and a piece-wise constant discontinuous field for the unknown force and moment vectors $\hat{\boldsymbol{T}}$ and $\hat{\boldsymbol{M}}$. This choice is known to prevent shear locking, see e.g. Saleeb and Chang (1987) and Chapelle and Bathe (2011). As a consequence, only one local model is required for each beam element. The local models are built with cubic approximation along the beam axis, and linear triangular elements on the cross section. The solid models are built with cubic tetrahedrons.

All the examples show a quadratic convergence rate both for the local cross-section problem and the global beam problem. As an example, Table 1 shows, for two different time steps, the residual norm of the global problem of Sec. 3.5.

All the simulations leverage the python interface of DOLFIN (Logg et al., 2012), a library developed within the FEniCS project (Alnæs et al., 2015).

Table 1: Global beam model convergence.

	Residual norm	
Iteration	$t = 0.2$	$t = 0.4$
0	0.5	0.5
1	0.00317	0.04223
2	0.00939	0.00108
3	0.004111	3.17E-06
4	0.000060	–

Although the use of the automatic differentiation and code generation capabilities of FEniCS simplified a lot the development of this proof-of-concept code, it is worth noting that special care is needed for dealing with finite rotations in DOLFIN, see Morandini (2017) for details. The already cited dolfin-adjoint library is an extension of DOLFIN, and was of great help in understanding how to actually implement the computation of the second derivative of the cross- section complementary strain energy.

3.1. Elastic bent beam

A 10 mm long beam, with a 1×1 mm square cross section lying in the global $z - y$ plane is clamped at one extremity and loaded by a 10 N force in the z direction at its other extremity. Two different materials are considered; the first one is a Green-elastic material for which $\boldsymbol{S} = 2\mu\boldsymbol{\epsilon} + \lambda\boldsymbol{\epsilon} : \boldsymbol{I} \otimes \boldsymbol{I}$, with $\mu = E/(2(1+\nu))$ and $\lambda = E\nu/((1+\nu)(1-2\nu))$; the second one is a Neo-Hookean material with internal energy per unit of reference volume $w = \frac{\mu}{2}(I_1 - 3) + \frac{K_0}{2}(J-1)^2$, where $\mu = E/(2(1+\nu))$, $\lambda = E\nu/((1+\nu)(1-2\nu))$, $K_0 = E/(3(1-2\nu))$, $J = \det(\boldsymbol{F})$, $I_1 = J^{-2/3}(\boldsymbol{F}^T\boldsymbol{F}) : \boldsymbol{I}$. The Elastic modulus

and Poisson coefficient are $E = 1\,\mathrm{MPa}$ and $\nu = 0.33$, respectively, so that for infinitesimal deformations the material response is equal. Figure 2 compares the loaded-point displacement components obtained by the present approach (HR), a three dimensional model (3D) and an Abaqus beam model. The load is linearly increased up to the final value for $t = 1$, and then decreased down to zero for $t = 2$; this allows to verify that the models are free from any spurious residual strain after a cycle of deformation. Both beam models are built with ten elements, while the three dimensional model is built with a $10 \times 10 \times 20$ mesh of second-order tetrahedral elements. The three models do agree reasonably well, with the two-level beam a little bit less stiff. Figure 3 shows the deformed configuration reached at $t = 1$ by the 3D and HR beam models.

Figure 4 allows to compare the loaded-point displacement components obtained by the present approach with piece-wise constant discontinuous fields for the unknown force and moment vectors $\hat{\boldsymbol{T}}$ and $\hat{\boldsymbol{M}}$ (HR) and by the present approach but with piecewise linear discontinuous fields for the unknown force and moment vectors $\hat{\boldsymbol{T}}$ and $\hat{\boldsymbol{M}}$ (HR 1). The linear unknown force and moment vectors proves to be stiffer; furthermore, the computational time is almost doubled, since this approach do require the definition of two independent cross-section models for each beam element. Figure 5 shows the deformed configuration reached at $t = 1$ by the HR and HR 1 models.

When considering the Neo-Hookean material the Abaqus beam model seems unable to converge. Figure 6 compares the displacement obtained with the Neo-Hookean and the Green-elastic materials. While the displacement of the Green-elastic and Neo-Hookean beams is practically the same, the

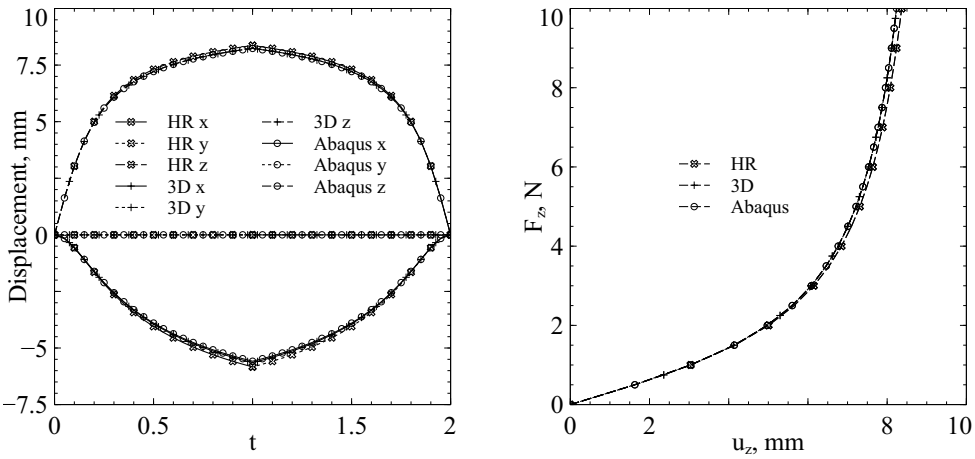

Figure 2: Green-elastic bent beam: loaded point displacement components as a function of time (left) and corresponding load-displacement curve (right).

root cross-section deformation and normal stress do differ, as it is clear from Figure 7.

3.2. Elasto-plastic bent beam

The beam of Sec. 3.1, 10 mm long and with a 1×1 mm square cross section, is now assumed to be made with an elasto-plastic isotropic material. The constitutive law is based on an additive decomposition of the Green-Lagrange strain tensor is $\boldsymbol{S} = \mathbb{E} : (\boldsymbol{\epsilon} - \boldsymbol{\epsilon}_p)$, where $\boldsymbol{\epsilon}_p$ is the plastic deformation tensor; a standard Von-Mises yield function f with isotropic hardening

$$f = \sqrt{\frac{3}{2}\boldsymbol{s} : \boldsymbol{s}} - (S_0 + K) = 0 \tag{27}$$

is assumed, with $\boldsymbol{s} = \boldsymbol{S} - \frac{1}{3}\boldsymbol{S} : \boldsymbol{I}$, S_0+K the equivalent yield stress. The internal energy is

$$\psi(\boldsymbol{\epsilon}, \boldsymbol{\chi}) = \frac{1}{2}(\boldsymbol{\epsilon} - \boldsymbol{\epsilon}_p) : \mathbb{E} : (\boldsymbol{\epsilon} - \boldsymbol{\epsilon}_p) + \frac{1}{2} H \boldsymbol{\epsilon}_p^{eff} \boldsymbol{\epsilon}_p^{eff}$$

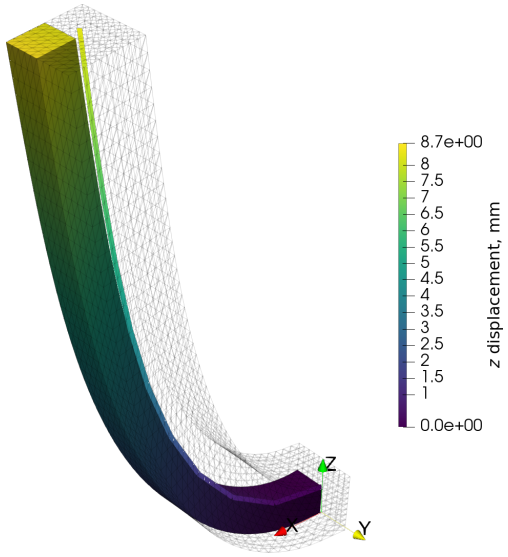

Figure 3: Green-elastic bent beam: overall displacement of the 3D model (wireframe, with only one quarter rendered as solid) and of the HR beam (colored line).

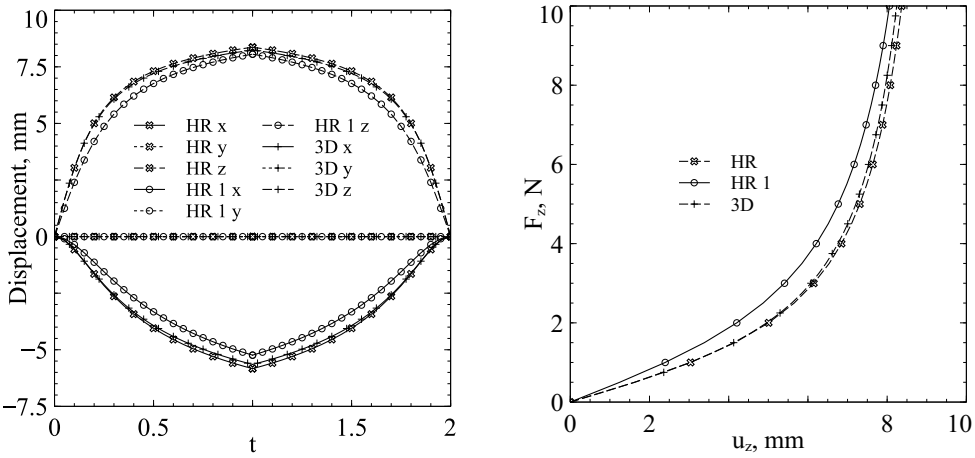

Figure 4: Green-elastic bent beam: comparison between beam elements with internal actions unknowns constant over each element (HR) and computed independently for the two integration points (HR 1); loaded point displacement components as a function of time (left) and corresponding load-displacement curve (right); .

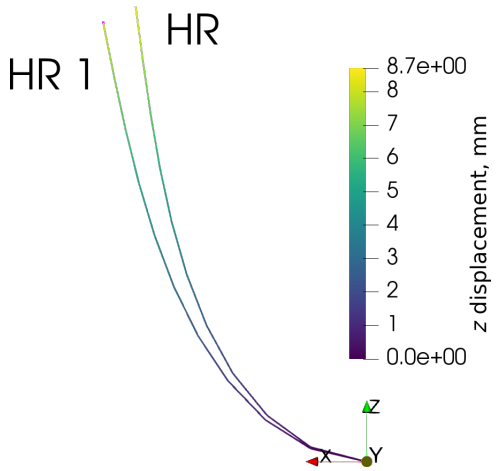

Figure 5: Green-elastic bent beam: overall displacement comparison between beam elements with internal actions unknowns constant over each element (HR) and computed independently for the two integration points (HR 1).

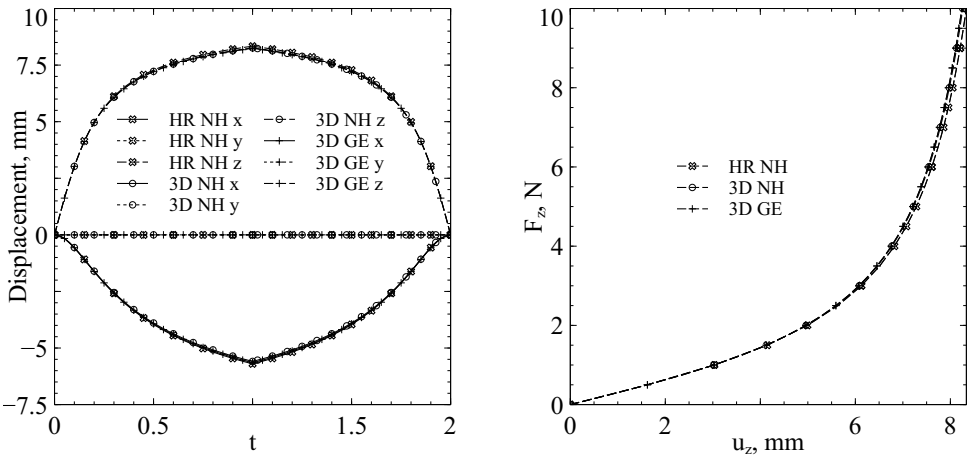

Figure 6: Neo-Hookean bent beam: loaded point displacement components as a function of time (left) and corresponding load-displacement curve (right).

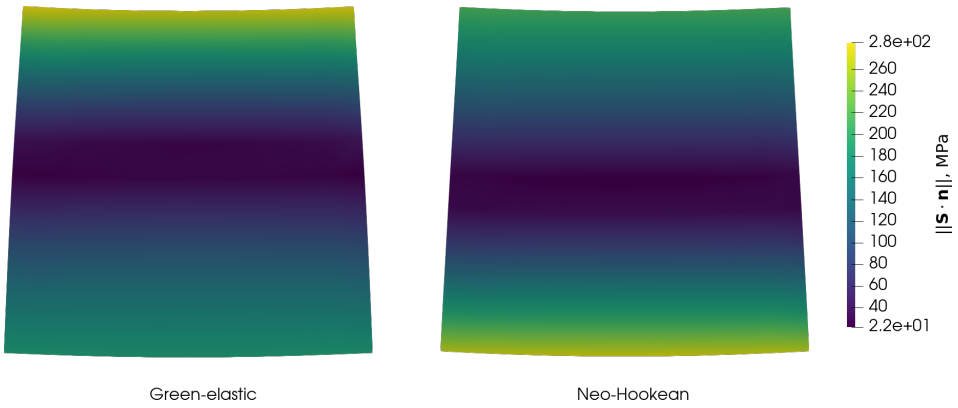

Figure 7: Green-elastic (left) and Neo-Hookean (right) root cross-section: deformed shape and norm of the normal stress vector.

and as associated flow rule is assumed. The elastic modulus and Poisson coefficient are $E = 1200\,\text{MPa}$ and $\nu = 0.3$, the yield stress is $S_0 = 12$ MPa, and the hardening parameter is $H = E_t/(1 - E_t/E)$ where $E_t = 360\,\text{MPa}$ is the tangent elasto-plastic modulus. The beam, clamped at one extremity, is subject to a transverse force of 1 N in the z direction; after reaching its maximum value for $t = 1$ the load is subsequently decreased to zero for $t = 2$. The loaded point displacements is in agreement with those obtained both using a three dimensional model and an Abaqus beam model with an elasto-plastic constitutive law.

3.3. Elasto-plastic L-shaped beam

A 5×10 mm L-shaped beam, with the same cross-section and material properties and Sec. 3.2 is clamped at one extremity and subject to a vertical transverse force of 1 N at the other extremity. This test case allows to verify the proposed approach soundness for bent and twisted beams, and leads to the deformed shapes of Fig. 9. The loaded point displacements are again in

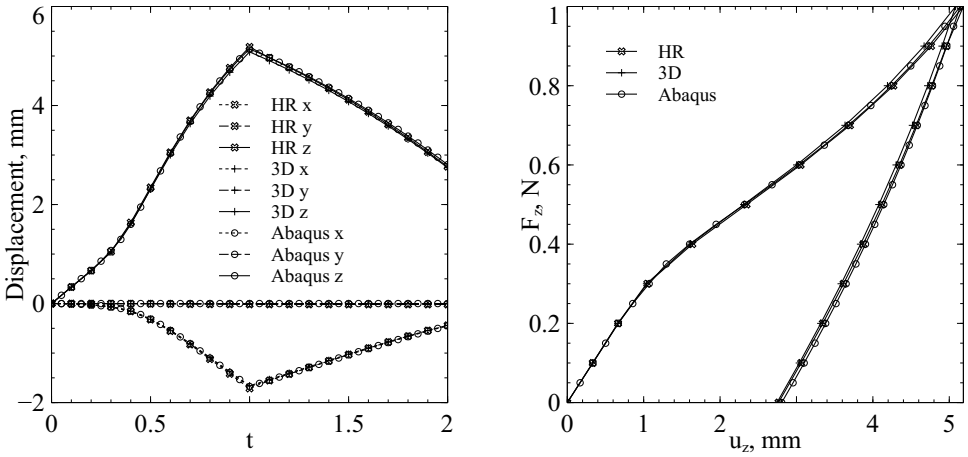

Figure 8: Elasto-elastic bent beam: loaded point displacement components as a function of time (left) and corresponding load-displacement curve (right).

good agreement with those of a three dimensional model and of an Abaqus beam model, as shown in Fig. 10.

3.4. Bimetallic beam

A straight beam of length 10 mm has the bimetallic 1×1 mm cross-section of Fig. 11 and is loaded by a transverse force F=1 N at its extremity. Both materials are defined by the elasto-plastic constitutive law of Sec. 3.2, with E=1200 MPa, $\nu = 0.3$ and $E_t = 360\,\text{MPa}$; the two material yield stresses do differ, and is equal to $S_0 = 2.4$ MPa and $S_0 = 12$ MPa for materials Mat. 1 and Mat. 2, respectively. Figure 12 compares the beam model loaded point displacement with that o a three dimensional simulation. Figures 13 and 14 plot the root section equivalent plastic strain and the norm of the normal stress vector, respectively. As expected, the left half of the beam, made with Mat. 1, undergoes a significant plastic deformation, with the normal stress vector limited to values that are smaller than those of the right half of the

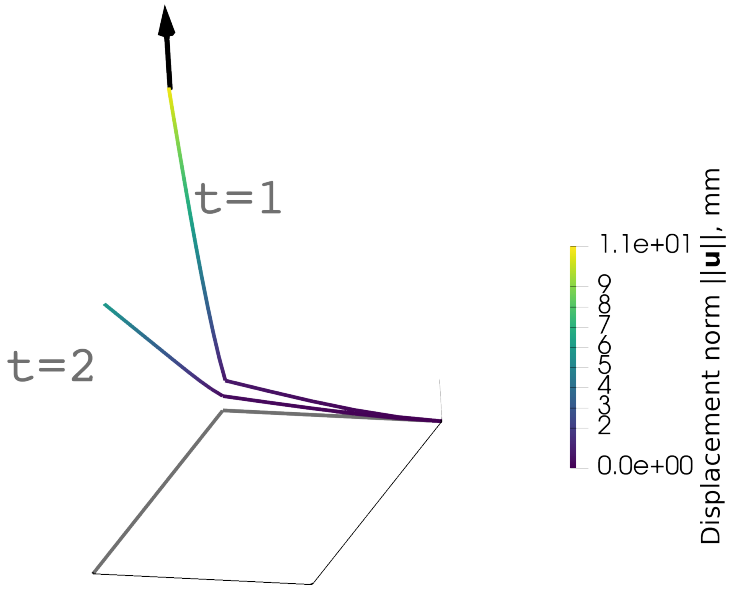

Figure 9: Elasto-plastic L-shaped beam deformed configurations.

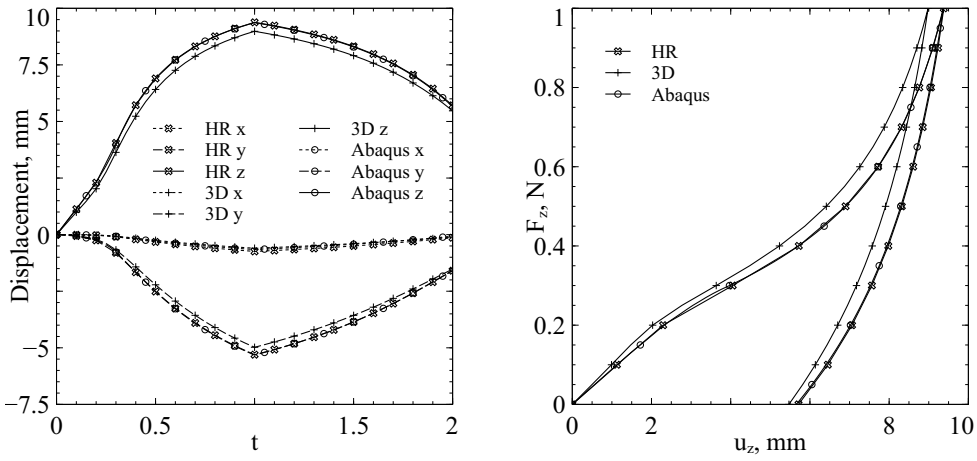

Figure 10: Elasto-plastic L-shaped beam: loaded point displacement components as a function of time (left) and corresponding load-displacement curve (right).

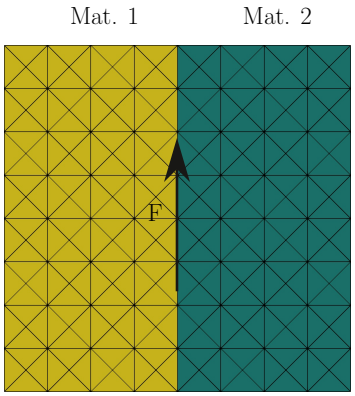

Figure 11: Bimetallic beam cross-section.

beam, that is made with Mat. 2.

3.5. Complex cross-section

A circular composite PVC wire of length $l = 10$ mm is discretized with 10 beam elements. It has a circular cross-section with a radius $R = 0.5$ mm and 19 smaller copper wires, each of radius $r = 0.08$ mm, as shown in Fig. 15. The PVC is assumed to be elastic, while the copper is elasto-plastic. The material properties are reported in Table 2. The cross-section mesh is made of 2527 triangular linear elements, with 1326 vertices and an average element size of 0.03 mm.The beam, clamped at one end, is subject to a concentrated shear force $F = 5$ N at the other extremity.The load is increased linearly from $t = 0$ to $t = 1$, and them brought to 0 for $t = 2$. This example requires a somewhat refined cross-section mesh, with a typical element dimension much smaller than what is required along the beam axis. A three dimensional mesh with well-shaped constant stress tetrahedron would require about 450 thousand nodes, for about 1.5 million unknowns, and is out of reach on the desktop computer used for these computations.

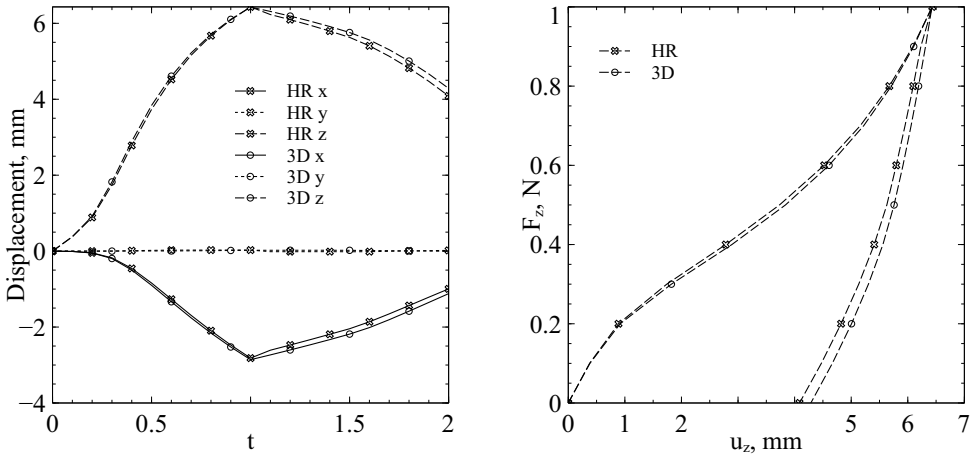

Figure 12: Dual material elasto-plastic beam: loaded point displacement components as a function of time (left) and corresponding load-displacement curve (right).

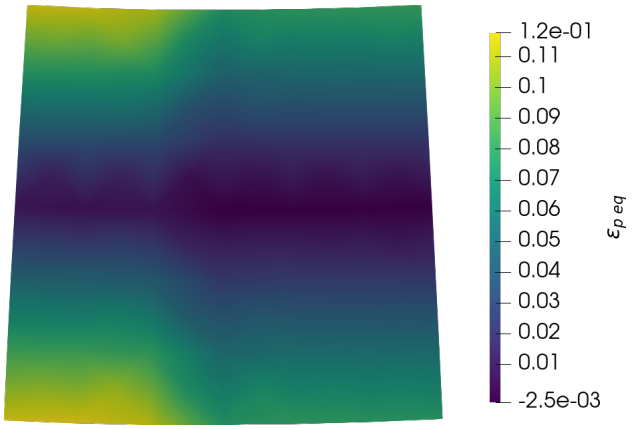

Figure 13: Dual material elasto-plastic beam: equivalent plastic deformation at $t = 1$.

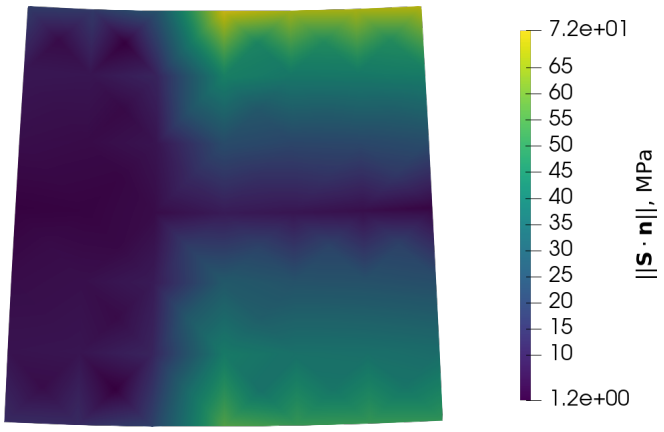

Figure 14: Dual material elasto-plastic beam: norm of the normal stress vector at $t = 1$.

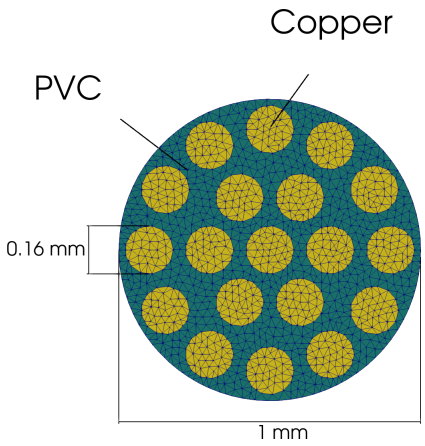

Figure 15: Mesh of the composite wire.

Table 2: Composite wire material properties.

	Copper	PVC
E	117 GPa	4.1 GPa
ν	0.3	0.41
S_0	70 MPa	/
E_t	2.34 GPa	/

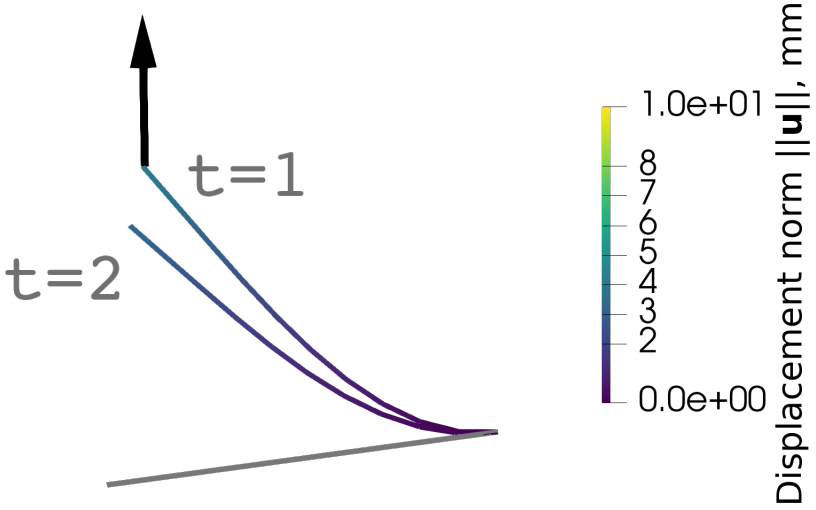

Figure 16: Elasto-plastic wire beam deformed configurations.

Figure 16 plots the deformed configuration taken by the beam when the load reaches it maximum at $t = 1$ and after unloading the structure, at $t = 2$. The corresponding beam tip displacement components are reported in Fig. 17, where x is along the beam axis and the load is applied in the z direction. Figures 18 plot the deformed root cross-section, with the colors representing the cross-section out of plane displacement for the fully loaded ($t = 1$, left) and unloaded ($t = 2$, right) configurations; it is worth noting how the cross-section depart from its planar reference shape,especially in the unloaded configuration. Figure 19 plots, instead, the equivalent plastic strain $\boldsymbol{\epsilon}_{peq}$ of the copper wires; the wires far away from the neutral axis undergo a significant plastic deformation, while the copper wires near the neutral axis are free from plastic deformations, as expected.

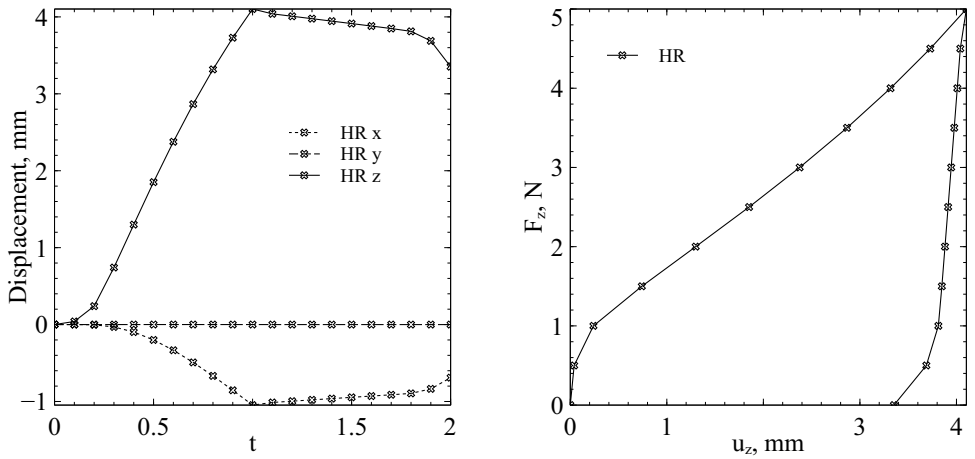

Figure 17: Elasto-plastic wire beam: loaded point displacement components as a function of time (left) and corresponding load-displacement curve (right).

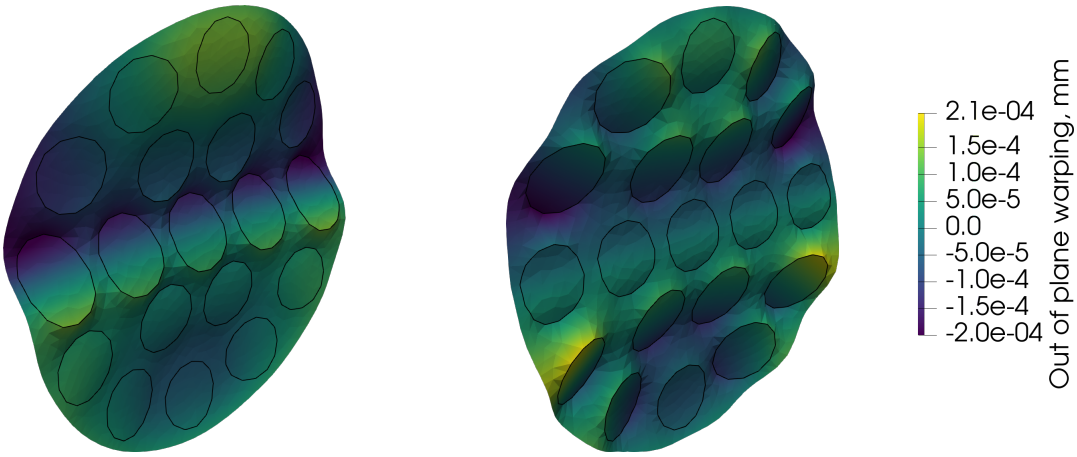

Figure 18: Composite wire out of plane warping, root element cross section: maximum load (left, $t = 1$) and final unloaded state (right, $t = 2$); deformation scale factor: 300.

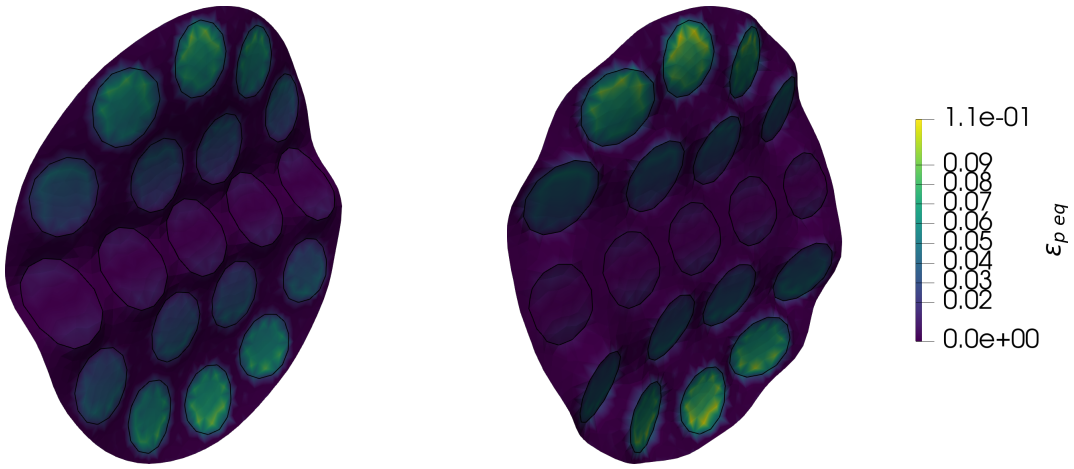

Figure 19: Composite wire equivalent plastic strain, root element cross section: maximum load (left, $t = 1$) and final unloaded state (right, $t = 2$); deformation scale factor: 300.

4. Run time

A few words about the run time requirements of the proposed two-level method are on order. As shown in Morandini (2019) the nonlinear analysis of a single cross-section easily outperforms a three dimensional analysis. This should not be a surprise, since the cross-section analysis is performed on a two-dimensional domain, thus with a drastically smaller number of unknowns wrt. that of a three dimensional model. Here, however, one needs many independent cross-section models, one for each beam element. Furthermore, at each and every iterations of the outer beam model one needs not only to solve the underlying cross-section nonlinear problem, but also to solve thirteen linear problems in order to compute the first and second order derivatives of the complementary strain energy. As a result, the run time of the three dimensional models and of the corresponding multi-level beam models turned out to be comparable for all the examples excluding the

Table 3: Timing comparison between the proposed approach and a fully three-dimensional solution.

		Section 10×10			Section 20×20			Section 40×40		
		Beam	3D	Ratio	Beam	3D	Ratio	Beam	3D	Ratio
Beam elements	10	1033 s	926 s	1.12	4112 s	5810 s	0.71	29540 s	51598 s	0.57
	20	1985 s	1751 s	1.13	8146 s	12793 s	0.63	/	/	/
	40	3741 s	3368 s	1.11	/	/	/	/	/	/

example of Sec. 3.5. The proposed approach is faster than a fully three dimensional analysis only if the spatial resolution required on the cross section is relatively high with respect the the resolution along the axis. A possible cross-over point could be that of the composite wire example of Sec. 3.5, or even that of more complex sections, for which a three dimensional model would require a significant effort. Table 3 compares the run time required by the Green-elastic bent beam of Sec. 3.1 for different cross-section and beam axis meshes. The analyses are performed with twenty load steps; following the benchmark results of Morandini (2019) a conjugated gradient with incomplete LU factorization as a preconditioner is chosen as the more efficient linear solver for the three-dimensional problem at hand. It is clear from the table that, for the same discretization along the axis, the proposed two-level approach becomes competitive only if the the cross-section mesh has a significant number of elements, and that the potential saving increases together with the number of the cross-section elements. The $40 \times 20 \times 20$, $20 \times 40 \times 40$ and $40 \times 40 \times 40$ table entries are missing because of the limited memory of the computer at hand.

5. Conclusions

The proposed two-level analysis procedure is able to deal with the non-linear response of non-homogeneous cross-sections, with arbitrary material constitutive laws, be them either elastic, hyperelastic or elasto-plastic. The proposed approach, with its somewhat high computational cost, is not competitive with classic kinematic approaches whenever it is reasonable to assume an axial stress state and it is possible to rephrase the constitutive law for it. A typical example is the elasto-plastic response of a homogeneous cross-section made with isotropic elasto-plastic material of Subsection 3.2, for which ABAQUS's standard beam elements give the same response at a fraction of the computational time. Such standard beam finite elements, however, fail to deal with hyperelastic constitutive laws, and are limited to relatively simple cross-sections. Thus, the proposed approach can be one of the few viable approaches for very specific beam problems.

The main theoretical advantage of the proposed method is that the link between the beam and the cross-section model is not delegated to the cross-section deformation modes, that could change throughout the analysis due to the nonlinear material response, but to the resultant and moment resultant of the cross-section normal stress vector. These quantities have a clear definition and well-defined physical meaning. A consequence of this approach is that the overall beam response is guaranteed to be hyperelastic if the cross-section material is hyperelastic. This is because, for any given state of normal stress resultant and moment resultant $\{\hat{\boldsymbol{T}}, \hat{\boldsymbol{M}}\}$, the solution of the cross-section problem of Eq. 14 is independent from the deformation history if the material is hyperelastic. The drawback of the proposed for-

mulation clearly lies in its relatively high computational cost: not only the second-order adjoint of Subsection 2.4 is particularly expensive, but for each and every equilibrium iteration of the higher level model one needs to solve a nonlinear cross-section problem. One thing to note, however, is that each cross-section model is independent with respect to the others. Thus, it should be possible to achieve significant speedups by solving in parallel, with a process for each cross-section, first the nonlinear problem and then the first and second order adjoint problems.

References

Alnæs, M.S., Blechta, J., Hake, J., Johansson, A., Kehlet, B., Logg, A., Richardson, C., Ring, J., Rognes, M.E., Wells, G.N., 2015. The fenics project version 1.5. Archive of Numerical Software 3. doi:10.11588/ans.2015.100.20553.

Berdichevsky, V.L., 1981. On the energy of an elastic rod. Journal of Applied Mathematics and Mechanics 45, 518–529. URL: http://www.sciencedirect.com/science/article/B6V3R-4805K2G-356/2/0a31717f1ca9fc8 doi:doi: DOI: 10.1016/0021-8928(81)90097-6.

Bilotta, A., Garcea, G., 2019. A two-level computational approach for the elasto-plastic analysis of framed structures with composite cross-sections. Composite Structures 209, 192–205. URL: http://www.sciencedirect.com/science/article/pii/S0263822318321998, doi:10.1016/j.compstruct.2018.10.056.

Bîrsan, M., Altenbach, H., Sadowski, T., Eremeyev, V.A., Pietras, D.,

2012. Deformation analysis of functionally graded beams by the direct approach. Composites Part B: Engineering 43, 1315–1328. URL: http://www.sciencedirect.com/science/article/pii/S1359836811004185, doi:10.1016/j.compositesb.2011.09.003.

Cardona, A., Geradin, M., 1988. A beam finite element non-linear theory with finite rotations. Int. J. Numer. Meth. Engng 26, 2403–2438.

Chapelle, D., Bathe, K.J., 2011. The Finite Element Analysis of Shells - Fundamentals. Computational Fluid and Solid Mechanics. 2 ed., Springer-Verlag, Berlin Heidelberg. URL: https://www.springer.com/gp/book/9783642164071, doi:10.1007/978-3-642-16408-8.

Chiorean, C.G., 2017. Second-order flexibility-based model for nonlinear inelastic analysis of 3d semi-rigid steel frameworks. Engineering Structures 136, 547–579. URL: http://www.sciencedirect.com/science/article/pii/S0141029617301992, doi:10.1016/j.engstruct.2017.01.040.

Druz, A.N., Polyakov, N.A., Ustinov, Y.A., 1996. Homogeneous solutions and Saint-Venant problems for a naturally twisted rod. Journal of Applied Mathematics and Mechanics 60, 657–664.

Farrell, P., Ham, D., Funke, S., Rognes, M., 2013. Automated Derivation of the Adjoint of High-Level Transient Finite Element Programs. SIAM Journal on Scientific Computing 35,

C369–C393. URL: https://epubs.siam.org/doi/10.1137/120873558, doi:10.1137/120873558.

Genoese, A., Genoese, A., Bilotta, A., Garcea, G., 2014a. A composite beam model including variable warping effects derived from a generalized Saint Venant solution. Composite Structures 110, 140–151. URL: http://www.sciencedirect.com/science/article/pii/S0263822313006107, doi:10.1016/j.compstruct.2013.11.020.

Genoese, A., Genoese, A., Bilotta, A., Garcea, G., 2014b. A generalized model for heterogeneous and anisotropic beams including section distortions. Thin-Walled Structures 74, 85–103. URL: http://www.sciencedirect.com/science/article/pii/S0263823113002413, doi:10.1016/j.tws.2013.09.019.

Giavotto, V., Borri, M., Mantegazza, P., Ghiringhelli, G.L., Carmaschi, V., Maffioli, G.C., Mussi, F., 1983. Anisotropic beam theory and applications. Computers & Structures 16, 403–413.

Han, S., Bauchau, O.A., 2015. On Saint-Venant's Problem for Helicoidal Beams. Journal of Applied Mechanics 83, 021009–021009. URL: http://dx.doi.org/10.1115/1.4031935, doi:10.1115/1.4031935.

Hinze, M., Pinnau, R., Ulbrich, M., Ulbrich, S., 2008. Optimization with PDE Constraints. 2009 edition ed., Springer, Dordrecht.

Hodges, D.H., 2006. Nonlinear composite beam theory. Number 213 in Progress in Astronautics and Aeronautics, American Institute of Aeronau-

tics and Astronautics, 1801 Alexander Bell Drive, Suite 500, Reston, VA, 20191-4344, USA.

Ieşan, D., 1976. Saint-Venant's problem for inhomogeneous and anisotropic elastic bodies. Journal of Elasticity 6, 277–294. URL: https://doi.org/10.1007/BF00041722, doi:10.1007/BF00041722.

Ieşan, D., 2008. Classical and Generalized Models of Elastic Rods. CRC Press.

Jiang, F., Yu, W., 2015. Nonlinear Variational Asymptotic Sectional Analysis of Hyperelastic Beams. AIAA Journal URL: https://arc.aiaa.org/doi/10.2514/1.J054334, doi:10.2514/1.J054334.

Logg, A., Wells, G.N., Hake, J., 2012. DOLFIN: a C++/Python Finite Element Library. Springer. chapter 10.

Merlini, T., Morandini, M., 2013. On successive differentiations of the rotation tensor: An application to nonlinear beam elements. Journal of Mechanics of Materials and Structures 8, 305–340. URL: https://msp.org/jomms/2013/8-5/p03.xhtml, doi:10.2140/jomms.2013.8.305.

Mielke, A., 1991. Hamiltonian and Lagrangian Flows on Center Manifolds with Applications to Elliptic Variational Problems. volume 1489 of *Lecture Notes in Mathematics*. Springer Berlin / Heidelberg. doi:10.1007/BFb0097544.

Mitusch, S., Funke, S., Dokken, J., 2019. dolfin-adjoint 2018.1: automated adjoints for FEniCS and Firedrake. Journal of Open Source Software 4, 1292. URL: https://joss.theoj.org/papers/10.21105/joss.01292, doi:10.21105/joss.01292.

Morandini, M., 2017. Handling of finite rotations in Dolfin, in: Proceedings of the FEniCS Conference 2017, Jack S. Hale, University of Luxembourg, Luxembourg. URL: http://dx.doi.org/10.6084/m9.figshare.5086369, doi:10.6084/m9.figshare.5086369.

Morandini, M., 2019. Analysis of beam cross section response accounting for large strains and plasticity. International Journal of Solids and Structures 176-177, 150–172. URL: http://www.sciencedirect.com/science/article/pii/S0020768319302471, doi:10.1016/j.ijsolstr.2019.05.014.

Morandini, M., Chierichetti, M., Mantegazza, P., 2010. Characteristic behavior of prismatic anisotropic beam via generalized eigenvectors. International Journal of Solids and Structures 47, 1327–1337. URL: http://www.sciencedirect.com/science/article/pii/S0020768310000284, doi:10.1016/j.ijsolstr.2010.01.017.

Pietraszkiewicz, W., Eremeyev, V.A., 2009. On natural strain measures of the non-linear micropolar continuum. Int. J. Solids Struct. 46, 774–787.

Rezaiee-Pajand, M., Gharaei-Moghaddam, N., 2015. Analysis of 3d Timoshenko frames having geometrical and material nonlinearities.

International Journal of Mechanical Sciences 94-95, 140–155. URL: http://www.sciencedirect.com/science/article/pii/S0020740315000685, doi:10.1016/j.ijmecsci.2015.02.014.

Rigobello, R., Breves Coda, H., Munaiar Neto, J., 2013. Inelastic analysis of steel frames with a solid-like finite element. Journal of Constructional Steel Research 86, 140–152. URL: http://www.sciencedirect.com/science/article/pii/S0143974X13001016, doi:10.1016/j.jcsr.2013.03.023.

Romanova, N.M., Ustinov, Y.A., 2008. The Saint-Venant problem of the bending of a cylinder with helical anisotropy. Journal of Applied Mathematics and Mechanics 72, 481–488.

Saleeb, A.F., Chang, T.Y., 1987. On the hybrid-mixed formulation of C0 curved beam elements. Computer Methods in Applied Mechanics and Engineering 60, 95–121. URL: http://www.sciencedirect.com/science/article/pii/0045782587901319, doi:10.1016/0045-7825(87)90131-9.

Zubov, L.M., 2006. The non-linear Saint-Venant problem of the torsion, stretching and bending of a naturally twisted rod. Journal of Applied Mathematics and Mechanics 70, 300–310.